Validation of a Mid-Fidelity Approach for Aircraft Stability and Control Characterization

Benjamin M. Simmons* and Steven C. Geuther†
NASA Langley Research Center, Hampton, Virginia 23681

Vivek Ahuja‡
Research in Flight, Austin, Texas 78750

This paper describes an efficient computational approach for aircraft aerodynamic model development intended for use in flight dynamics simulations. A commercial surface-vorticity flow solver called FlightStream® is employed to predict performance, stability, and control characteristics for a NASA subscale electric vertical takeoff and landing aircraft in its isolated-airframe configuration. A framework is described to rapidly convert OpenVSP geometry into a form compatible with the FlightStream® software. FlightStream® predictions for the variation of aerodynamic force and moment coefficients with airflow angles and control surface deflection angles are compared to static wind-tunnel data to illustrate the process and assess the accuracy of FlightStream® solutions. The results and approach presented in this paper are encouraging for use in rapid aerodynamic modeling and flight dynamics simulation development early in the aircraft design process.

Nomenclature

b	=	wingspan, ft
C_L, C_D, C_Y	=	lift, drag, and side force coefficients
C_l, C_m, C_n	=	body-axis rolling, pitching, and yawing moment coefficients
$\bar{c}$	=	mean aerodynamic chord, ft
$\mathcal{L}$, $\mathcal{D}$, Y	=	lift, drag, and side force components, lbf
L, M, N	=	body-axis rolling, pitching and yawing moment components, ft·lbf
n_1, n_2,..., n_6	=	propeller rotational speeds, revolutions/s
p, q, r	=	body-axis angular velocity components, rad/s or deg/s
$\bar{q} = \frac{1}{2}\rho V^2$	=	freestream dynamic pressure, lbf/ft^2
S	=	wing reference area, ft^2
V	=	freestream velocity, ft/s
α	=	angle of attack, rad or deg
β	=	angle of sideslip, rad or deg
δ_{c_1}, δ_{c_2},..., δ_{c_6}	=	collective pitch angles, rad or deg
δ_{f_1}, δ_{f_2},..., δ_{f_6}	=	flaperon deflection angles, rad or deg
δ_{t_1}, δ_{t_2}, δ_{t_3}, δ_{t_4}	=	nacelle tilt angles, rad or deg
δ_r	=	rudder deflection angle, rad or deg
δ_s	=	stabilator deflection angle, rad or deg

*Research Engineer, Flight Dynamics Branch, MS 308, Member AIAA.
†Aerospace Engineer, Aeronautics Systems Engineering Branch, MS 238.
‡CEO, Research in Flight, Senior Member AIAA.

I. Introduction

Many complex distributed hybrid and electric propulsion aircraft have emerged to enable future Advanced Air Mobility (AAM) transportation missions [1–5]. There are many design concepts with a variety of mission profiles including vertical takeoff and landing (VTOL), short takeoff and landing (STOL), and conventional takeoff and landing (CTOL) configurations. Although the operational utility of distributed propulsion aircraft has great potential, there are many research areas that need to be addressed prior to introduction of these unique vehicles for AAM missions in the national airspace system. Vehicle technical challenges include: airworthiness certification, air traffic management, pilot-operator interface, handling qualities, simplified vehicle operations, contingency management, vehicle autonomy, and flight controls strategies. One important enabling tool for many research efforts is a vehicle flight dynamics simulation driven by an aero-propulsive model. Efficient and accurate aero-propulsive model development, however, is challenged by several vehicle attributes including: many control surfaces and propulsors, substantial propulsion-airframe interactions, and large flight envelopes that need to be characterized by a global aero-propulsive model.

Previous research has investigated methods for efficient full-envelope electric VTOL (eVTOL) aircraft aero-propulsive model development using computational fluid dynamics (CFD) simulations [6, 7] and wind-tunnel testing [8–13]. These techniques were successful in developing accurate aero-propulsive models well-suited for flight dynamics simulations of complex aircraft; however, they required time consuming CFD simulations with substantial subject matter expertise to effectively execute or the availability of a physical aircraft model and wind-tunnel test facility. Other related work has investigated using low-to-mid fidelity analytical and/or computational methods for developing dynamic models applicable for flight controls applications [14–19].

The present effort builds on this previous eVTOL aircraft modeling research to make progress towards developing an approach for rapid aero-propulsive model development using mid-fidelity computational experiments, allowing a flight dynamics model to be developed early in the aircraft design process. This paper specifically focuses on prediction of performance, stability, and control characteristics for a NASA subscale eVTOL aircraft in its isolated-airframe configuration (i.e., without propellers installed). Future work is expected to be expanded to powered-airframe studies focused on reduced order aero-propulsive model development suitable for flight dynamics simulations. Contributions of this paper include development of an approach enabling efficient computational prediction of vehicle aerodynamics and comparison of the results to static wind-tunnel data. FlightStream®, a commercial surface-vorticity flow solver developed by Research in Flight [20], is employed to compute aerodynamic forces and moments as a function of airflow angles, body-axis angular velocity, and control surface deflection angles which yields an isolated-airframe aerodynamic model suitable to perform flight simulations. FlightStream® has been used previously to develop aerodynamic predictions for aircraft with significant propeller-airframe interactions at a fraction of the expense of running CFD simulations [21–29]. FlightStream® has also been successfully applied to make aerodynamic predictions for numerous other aircraft configurations and components [30–41].

The paper is organized as follows: Section II introduces the research aircraft. Section III presents background information on the FlightStream® flow solver software. The process used to automatically execute FlightStream® simulations starting from OpenVSP geometry is outlined in Sec. IV. Comparisons of FlightStream® predictions to wind-tunnel data are shown in Sec. V. Overall conclusions are summarized in Sec. VI.

II. Aircraft

The modeling approach developed in this paper is applied to the Research Aircraft for eVTOL Enabling techNologies (RAVEN) Subscale Wind Tunnel and Flight Test (SWFT) model built at NASA Langley Research Center (LaRC). The RAVEN SWFT is a 28.625% scale version of the RAVEN 1000-lb eVTOL aircraft concept [42], which has been conceptualized as a collaborative effort between NASA LaRC and the Georgia Institute of Technology. The RAVEN aircraft is a tilt-rotor eVTOL aircraft configuration with six variable-pitch propellers. The front four propellers tilt forward and are operational throughout the entire flight envelope. The rear two propellers do not tilt and serve as lifting propellers in hover and transition. The rear propellers are inactive in forward flight. The aircraft control surfaces included six flaperons, an all moving stabilator, and a rudder. In total, the vehicle has 24 independent control effectors:

- Six propeller rotational speeds ($n_1, n_2, ..., n_6$)
- Six propeller collective pitch angles (δ_{c_1}, δ_{c_2},..., δ_{c_6})
- Four nacelle tilt angles (δ_{t_1}, δ_{t_2}, δ_{t_3}, δ_{t_4})
- Six flaperon deflection angles (δ_{f_1}, δ_{f_2},..., δ_{f_6})
- One stabilator deflection angle (δ_s)
- One rudder deflection angle (δ_r)

A schematic of the RAVEN aircraft with annotations showing the vehicle propulsor and control surface definitions is shown in Fig. 1. Flaperon and stabilator deflections are defined as positive trailing edge downward. Rudder deflection is defined as positive trailing edge left. As currently configured, propeller 1, 3, and 5 rotate counterclockwise and propeller 2, 4, and 6 rotate clockwise, as viewed from the perspective of each respective electric motor.

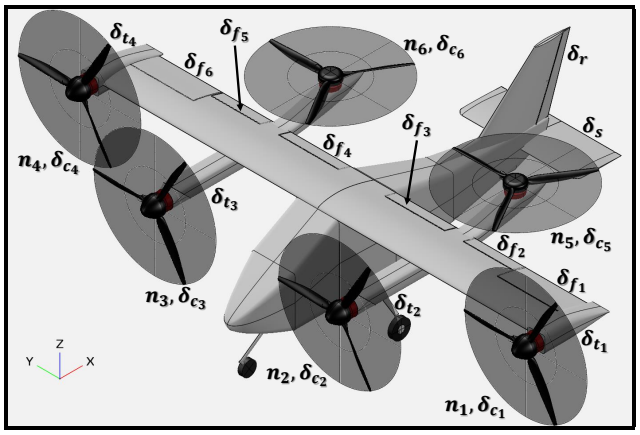

Fig. 1 RAVEN control effector definitions.

The RAVEN SWFT, pictured in the NASA Langley 12-Foot Low-Speed Tunnel (LST) [43] in Fig. 2, is a subscale aircraft configuration designed as a flight dynamics and controls testbed to advance eVTOL aircraft technology. As its name suggests, the vehicle is designed for use in both wind-tunnel and flight-test experiments. The RAVEN SWFT was

(a) Front view (cruise configuration)

(b) Overhead view (hover configuration)

(c) Side view (mid-transition configuration)

(d) Rear view (mid-transition configuration)

Fig. 2 RAVEN SWFT mounted in the NASA Langley 12-Foot Low-Speed Tunnel.
(Credit: Lee Pollard, NASA Langley Research Center)

developed at NASA LaRC as one of several subscale eVTOL research aircraft intended to explore their unique flight characteristics and resolve implementation challenges to help bring similar full-scale vehicles into mainstream operation. Previous aircraft have included the LA-8 [44, 45] and GL-10 [46], which have enabled research in computational aerodynamic predictions [27, 37], wind-tunnel testing [8, 11, 47], high incidence angle propeller aerodynamics [48–50], aero-propulsive modeling [9, 12, 13, 46, 51], flight controls [52, 53], and flight-test strategies [54–57].

Initial RAVEN SWFT wind-tunnel tests have been performed in the 12-Foot LST for the isolated 19.5-inch variable-pitch propeller [58], the isolated airframe (without propellers operating), and powered airframe (with propellers operating). RAVEN SWFT wind-tunnel data collected during the isolated airframe experiments is used as validation data for FlightStream® predictions shown later in the paper.

III. FlightStream® Background

The mid-fidelity flow solutions for this effort were performed using the FlightStream® viscous surface-vorticity flow solver. FlightStream® has been developed by Research in Flight [20] as a highly efficient compressible subsonic, three-dimensional viscous-coupled, surface-vorticity panel-method flow solver. FlightStream® allows for rapid analysis of unconventional aircraft in both powered and unpowered configurations. The FlightStream® flow solver has been developed under several NASA and USAF Small Business Innovation Research (SBIR) developmental contract awards [59–63].

FlightStream® makes use of the resolved surface-vorticity to compute aerodynamic load distributions using advanced Fast Multipole Method and wake proximity avoidance algorithms. These innovations allow FlightStream® to generate aerodynamic results in minutes for multirotor simulations using an unstructured surface mesh. FlightStream® works directly with commercial computer-aided design (CAD) software for its geometry input by merging the surface boundary conditions with the analytical CAD provided by the designer. FlightStream® also works with OpenVSP [64, 65] and The Engineering Sketch Pad [66]. As part of NASA SBIR work [59, 60], FlightStream® was expanded to allow for nonlinear aerodynamics, including unsteady flow, prediction of the onset of stall, $C_{L_{\max}}$, and post-stall aerodynamics. Key features of FlightStream® are summarized in Table 1.

Table 1 Summary of key FlightStream® features

1.	The use of unstructured surface meshes (volume meshing is not required).
2.	A subsonic, transonic, and supersonic panel-method solver capable of solutions in seconds.
3.	A Fast Multipole Method solver allowing very large mesh sizes solved in seconds-to-minutes with $O(n \log n)$ efficiency in the potential flow solver.
4.	Nonlinear solver capabilities which include models for the boundary layer and flow separation.
5.	A fully steady or unsteady time-domain solver.
6.	Advanced control surface modeling and flight control system integration capabilities.
7.	Fluid-structure interactions modeling with embedded static and dynamic aeroelastic, flutter, and aeroservoelastic modeling tools integrated with the core flow solvers.
8.	The ability to execute of six-degree-of-freedom (6DOF) motion simulations.
9.	A modern user interface/experience with a fully-scriptable application programming interface (API).
10.	Integration with commercial and open-source CAD software.

IV. Aerodynamic Modeling Approach

A new approach was formulated and applied to convert OpenVSP [64] geometry into a form compatible with the FlightStream® software [20]. This was followed by automatic execution of flow simulations using the FlightStream® scripting capabilities. The steps are as follows:

1) **Create an OpenVSP model for the aircraft geometry.** A RAVEN SWFT OpenVSP model in its cruise (forward flight) configuration was developed for this study. The vehicle components modeled in OpenVSP included the fuselage, main wing, horizontal tail, vertical tail, propellers, landing gear, inboard sponsons, outboard nacelles, and simplified representations of the electric motors. The model is a 28.625%-scale version of the

1000-lb RAVEN OpenVSP model with slight modifications made to emulate the as-built RAVEN SWFT aircraft geometry. The RAVEN SWFT OpenVSP model is shown in Fig. 3.

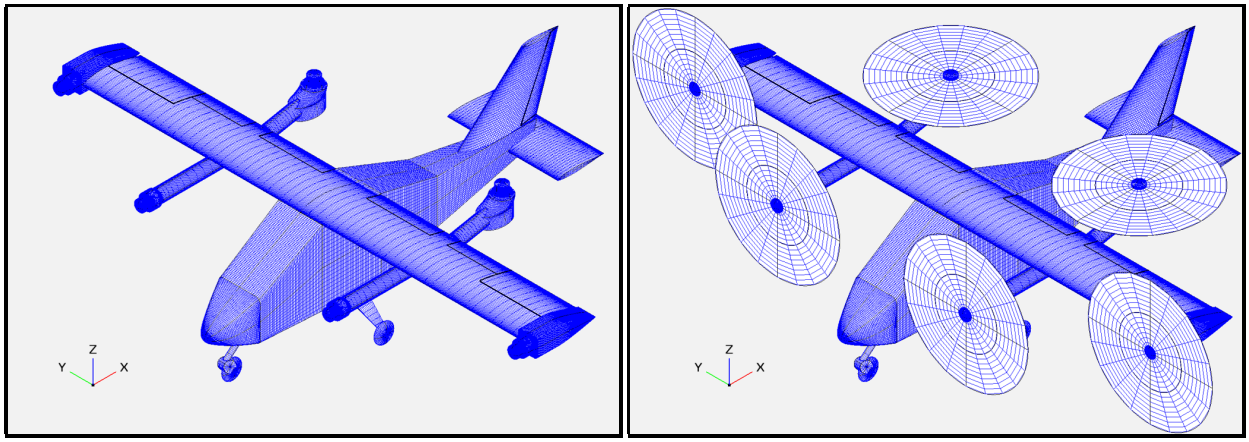

(a) Isolated airframe **(b) Powered airframe**

Fig. 3 RAVEN SWFT OpenVSP model.

2) **Adjust the tessellation and clustering for each component in the OpenVSP model.** The FlightStream® User Guide [67] contains guidance on how to set mesh controls for lifting and non-lifting components to facilitate successful grid generation in FlightStream®. Furthermore, it is important to ensure that the OpenVSP mesh resolution is finer than the mesh resolution used in FlightStream®.
3) **Export the aircraft geometry from OpenVSP by creating a degenerate geometry (DegenGeom) file.** For this work, the DegenGeom m-file export option was used to create a script that could be run in MATLAB®. The propeller components were not included in the DegenGeom file, but their locations were stored to be incorporated into the model later in the process.
4) **Convert the DegenGeom file into a Component Cross Section (CCS) file.** The CCS file, discussed in the FlightStream® User Guide [67], is a text file that allows the user to import aircraft geometry into FlightStream® in a manner suitable for automatic mesh generation. The CCS file also allows the user to define control surfaces and set several meshing options. For this work, a MATLAB® script was written to automatically convert the DegenGeom m-file into the CCS file format along with control surface positions and certain user-specified meshing parameters. The RAVEN SWFT isolated-airframe FlightStream® representation created from the CCS file is shown in Fig. 4.

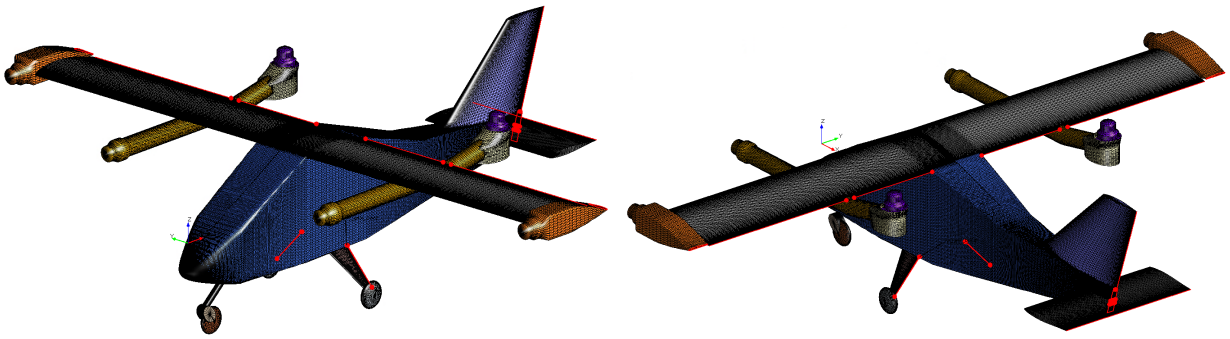

Fig. 4 RAVEN SWFT isolated-airframe FlightStream® mesh and boundary conditions.

5) **Perform a mesh refinement study.** Executing a mesh refinement study for each geometric component is an essential task to ensure that FlightStream® predictions are reliable and accurate. For each isolated component, the first step is to perform a mesh refinement study in the direction of the highest curvature, while holding the number of grid points in the lower curvature direction fixed to a reasonably dense value. The results have

sufficiently converged when the percent difference of the dominant force and moment components between neighboring grid refinement levels is less than 1-2%, which specifies the number of grid points that should be used for subsequent analyses. The second step is to perform a mesh refinement study in the lower curvature direction while holding the number of grid points in the higher curvature direction fixed to the value determined in the first step. For the most reliable results, the mesh refinement study should be performed at a non-zero angle of incidence relative to the oncoming flow (i.e., running the analysis at a non-zero angle of attack and angle of sideslip) and using the inviscid solver (i.e., viscous coupling and flow separation options should be disabled). For this work, the grid refinement was adjusted in a CCS file using the user-defined meshing parameters "Mesh_U" and "Mesh_V" [67]. The mesh refinement process is demonstrated for the RAVEN SWFT main wing in Fig. 5. A mesh refinement study is first performed in the chordwise direction by varying the number of chordwise grid points while holding the spanwise grid fixed at 40 points. Figure 5a shows that the percent difference of the C_L and C_m values is less than 1% using 200 chordwise points, which was selected as the number of chordwise grid points for the wing. A mesh refinement study was then performed in the spanwise direction holding the chordwise grid fixed at 200 points. As shown in Fig. 5b, the C_L and C_m values appear to sufficiently converge using 50 spanwise grid points.

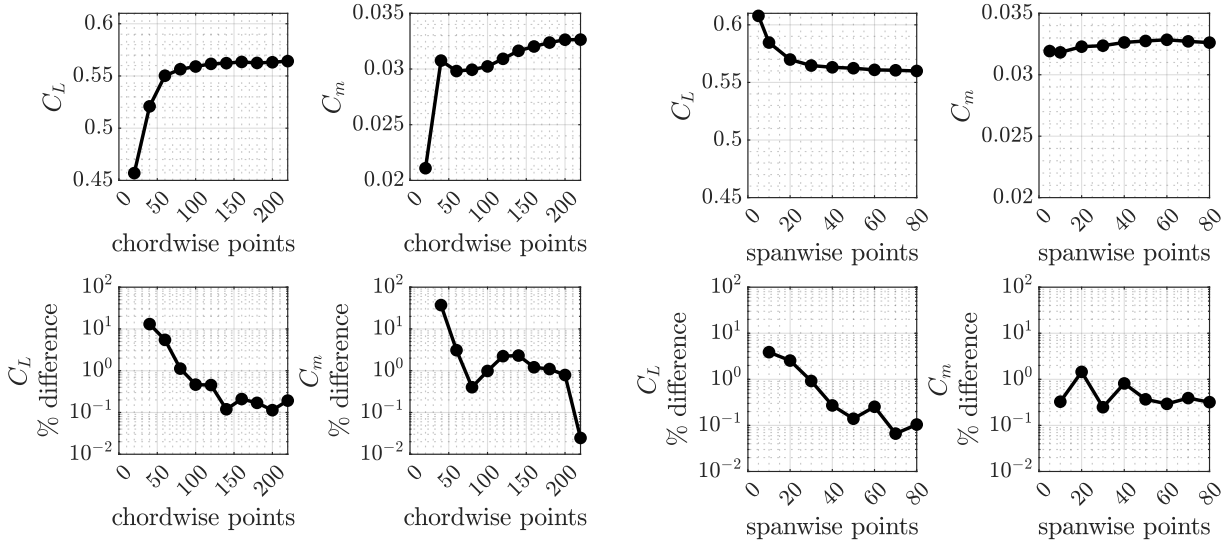

(a) Step 1: chordwise grid refinement (40 spanwise points) **(b) Step 2: spanwise grid refinement (200 chordwise points)**

Fig. 5 Mesh refinement study for the RAVEN SWFT wing (inviscid solver, α = 2 deg, β = 0 deg, V = 54.3 ft/s).

6) **Create FlightStream® script files to automatically execute simulations.** A MATLAB® script was written to automatically generate a FlightStream® script file for each simulation run. The FlightStream® script files were configured to perform tasks such as importing a CCS file, creating coordinate systems, creating propellers (modeled as Conway actuator discs [68]), specifying boundary conditions, setting flow solver options, setting control effector settings, running FlightStream® simulations, and saving results.
7) **Execute FlightStream® script files to generate aerodynamic predictions.** A MATLAB® script was written to automatically run a set of FlightStream® script files for automatic data generation for an arbitrary number of flow conditions and control effector settings. An example RAVEN SWFT powered-airframe FlightStream® flow solution visualization is shown in Fig. 6.

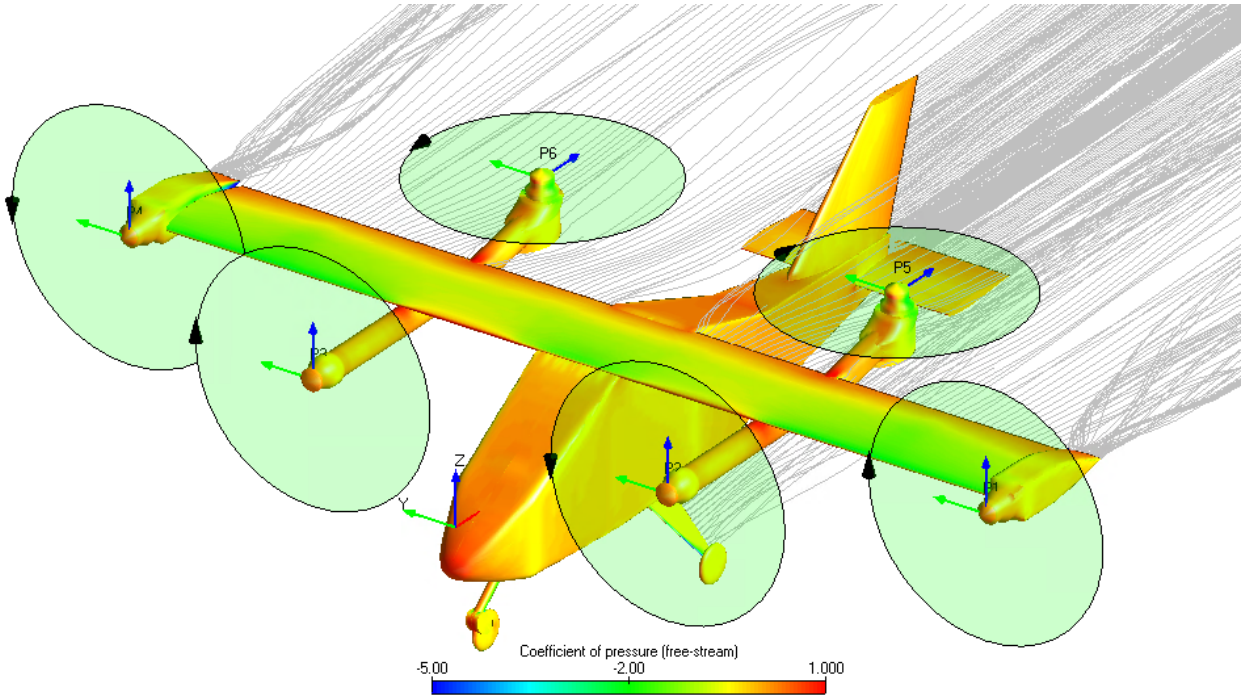

Fig. 6 Example powered-airframe FlightStream® surface pressure predictions for the RAVEN SWFT aircraft.

The set of procedures outlined in this section is summarized in Fig. 7. This process allows FlightStream® solutions to be run automatically at a variety of user-specified flight conditions for efficient prediction of applied forces and moments which can be used for aerodynamic database development.

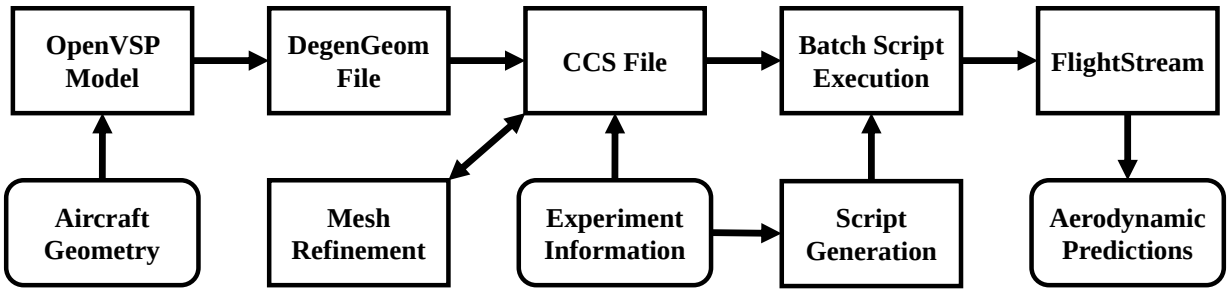

Fig. 7 Process to execute FlightStream® simulations.

V. Results

To demonstrate and validate the approach outlined in the previous section, FlightStream® was used to compute predictions of the isolated-airframe performance, stability, and control characteristics for the RAVEN SWFT aircraft. This includes computing the nondimensional aerodynamic force coefficients

$$C_L = \frac{\mathcal{L}}{\bar{q}S}, \quad C_D = \frac{\mathcal{D}}{\bar{q}S}, \quad C_Y = \frac{Y}{\bar{q}S}$$

and moment coefficients

$$C_l = \frac{L}{\bar{q}Sb}, \quad C_m = \frac{M}{\bar{q}S\bar{c}}, \quad C_n = \frac{N}{\bar{q}Sb}$$

variation with angle of attack, angle of sideslip, angular rates, and control surface deflection angles. The current estimated RAVEN SWFT forward flight center of gravity position was used as the moment reference location. Several

comparisons of FlightStream® predictions to wind-tunnel data collected for the RAVEN SWFT aircraft were made to validate FlightStream® solutions and determine suitable FlightStream® settings for modeling the RAVEN SWFT aircraft. FlightStream® solutions were run with a fully turbulent boundary layer and the pressure-based calculations were taken as the final results. Inviscid solutions were run for all cases; furthermore, angle of attack and angle of sideslip sweeps were performed with Stratford flow separation models enabled [59]. For this paper, the FlightStream® solutions were executed with the viscous coupling option disabled. FlightStream® Build #3092023 was used to compute the results shown in this paper.

The static wind-tunnel data used for validation of the FlightStream® solutions were collected using randomized test factor sweeps and statistically designed experiments (e.g., see Refs. [69, 70]) varying the airflow angles and control surface deflection angles. The data were collected in this manner to quantify the uncertainty of the wind-tunnel measurements and enable development of a response surface equation (RSE) for each aerodynamic force and moment component. Note that the randomized data collection strategy is intended to expose and characterize the uncertainty in the measured data and, consequently, makes the raw data quality look noisier than a traditional one-factor-at-a-time sweep where a single test factor is varied by sequentially increasing or decreasing its value. The wind-tunnel data are plotted as individual data points with repeat points shown where available to convey the magnitude of the measurement uncertainty. The wind-tunnel data are also displayed in the form of RSE predictions of the mean response along with a 95% confidence interval (CI) on the mean response and a 95% prediction interval (PI) characterizing the uncertainty in the response predictions for individual data points [70]. All wind-tunnel data were collected at a dynamic pressure of $\bar{q} = 3.5$ psf (freestream velocity of $V = 54.3$ ft/s at standard sea level conditions) and, accordingly, the FlightStream® solutions were run at these freestream settings.

A. Angle of Attack and Sideslip Sweep Predictions

Figure 8 shows FlightStream® predictions and wind-tunnel measurements of the lift, drag, and pitching moment coefficients for an angle of attack sweep at $\beta = 0$ deg. The results for two types of FlightStream® flow simulations are shown: an inviscid flow simulation and a flow simulation including the effects of flow separation (using the FlightStream® axial flow separation setting for the wing and horizontal tail, and the FlightStream® longitudinal crossflow setting for the fuselage and sponsons). The lift coefficient variation with angle of attack is well captured by both FlightStream® solutions below stall. The solution with flow separation modeled accurately predicts the stall location and maximum lift coefficient, as a result of employing the axial flow separation model on the wing and horizontal tail. The overall drag coefficient is underpredicted by the inviscid model, but the curvature matches the wind-tunnel data reasonably well. Below stall, the solution including flow separation effects better approximates the drag variation with angle of attack. This improvement was primarily gained by employing the longitudinal crossflow model for the fuselage and sponsons. The post-stall drag increase exhibited in the wind-tunnel data is not captured by either FlightStream® solution. The

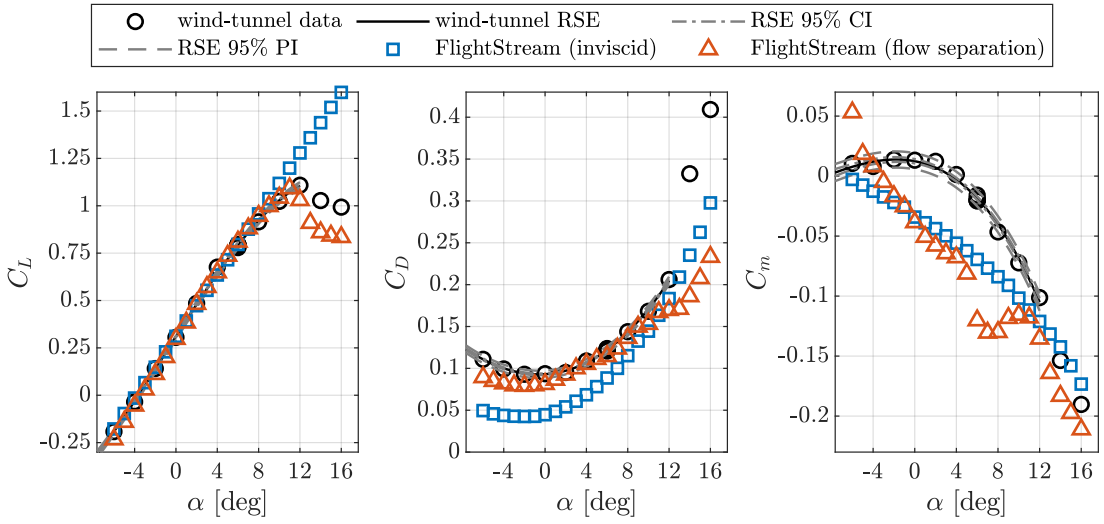

Fig. 8 Angle of attack sweep at $\bar{q} = 3.5$ psf ($V = 54.3$ ft/s), $\beta = 0$ deg, and zero control surface deflection.

pitching moment variation with angle of attack is reasonably well predicted by the inviscid FlightStream® solution for an angle of attack greater than approximately 2 deg. The solution with flow separation includes non-physical nonlinear behavior in the angle of attack range of 5 to 11 deg as a result of non-smooth introduction of the flow separation models, which is expected to be addressed and improved in a future version of FlightStream®. Furthermore, both FlightStream® solutions do not capture the decreasing stability, and eventual instability, of the pitching moment slope exhibited in the wind-tunnel data at a negative angle of attack. Resolving this discrepancy will be the subject of future work.

Figure 9 shows FlightStream® predictions and wind-tunnel measurements of side force, rolling moment, and yawing moment coefficients for an angle of sideslip sweep at $\alpha = 2$ deg. To aid in comparison of the FlightStream® results and wind-tunnel measurements, small asymmetries in the lateral-directional force and moment measurements have been removed by subtracting the force and moment values at $\beta = 0$ deg from all of the data. Two FlightStream® flow solutions are shown: an inviscid solution and a solution computed using the crossflow flow separation model enabled on the fuselage. For C_Y, the FlightStream® solution with flow separation well-represents the measured wind-tunnel data; the inviscid FlightStream® solution predicts a slope that is lower in magnitude compared to the wind-tunnel data. For C_l, both FlightStream® model predictions agree well with the wind-tunnel data, with the inviscid solution slightly more closely following the mean response predicted by the RSE. For C_n, the inviscid FlightStream® model exhibits a better match to the wind-tunnel data compared to the model with flow separation enabled, which overpredicts the yaw stiffness.

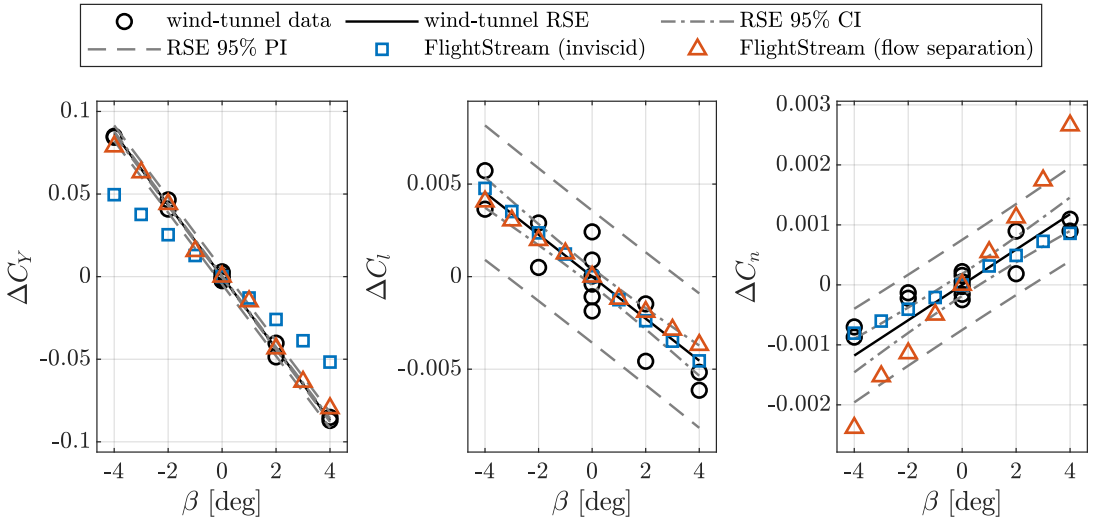

Fig. 9 Angle of sideslip sweep at $\bar{q} = 3.5$ psf ($V = 54.3$ ft/s), $\alpha = 2$ deg, and zero control surface deflection.

The α and β stability derivatives at $\alpha = 2$ deg and $\beta = 0$ deg computed from the wind-tunnel-derived RSEs and FlightStream® predictions using a smoothed polynomial representation of the data are shown in Table 2. The inviscid FlightStream® stability derivative predictions are closer to the wind-tunnel derived values compared to the flow separation model predictions, except for C_{Y_β} where the flow separation model prediction is closer to the wind-tunnel-derived value.

Table 2 Comparison of static stability derivatives at $\bar{q} = 3.5$ psf ($V = 54.3$ ft/s), $\alpha = 2$ deg, and $\beta = 0$ deg

Parameter	Wind Tunnel	FlightStream (inviscid)	FlightStream (flow separation)
C_{L_α}	+4.39	+4.64	+5.10
C_{D_α}	+0.214	+0.342	+0.353
C_{m_α}	-0.271	-0.312	-0.413
C_{Y_β}	-1.24	-0.737	-1.21
C_{l_β}	-0.0650	-0.0685	-0.0593
C_{n_β}	+0.0169	+0.0137	+0.0289

B. Control Surface Effectiveness Predictions

Each of the control surfaces were modeled in FlightStream® by specifying their geometry in the CCS file and executing geometry rotation commands in the FlightStream® script files where applicable. Because the aircraft has an all-moving stabilator, the stabilator deflections were modeled by rotating the whole horizontal tail component about its hinge point. The flaperon and rudder control surfaces were modeled using two different approaches possible in FlightStream®: morphing control surfaces and physically separating/deflecting control surfaces, which are depicted in Fig. 10a and Fig. 10b, respectively. The morphing surface approach rotates the surface about its hinge location which stretches the mesh and maintains a continuous trailing edge on the lifting surface. The separated surface approach results in a gap between the deflected control surface and lifting surface with a separate trailing edge on each component. To expedite the FlightStream® computations, the stabilator predictions were run without the landing gear, sponsons, motor representations, and nacelles. Similarly, the rudder and flaperon FlightStream® solutions were computed by only including the vertical tail and main wing components, respectively. Only inviscid FlightStream® solutions at $\alpha = 2$ deg and $\beta = 0$ deg were executed for the control surface predictions shown in this paper.

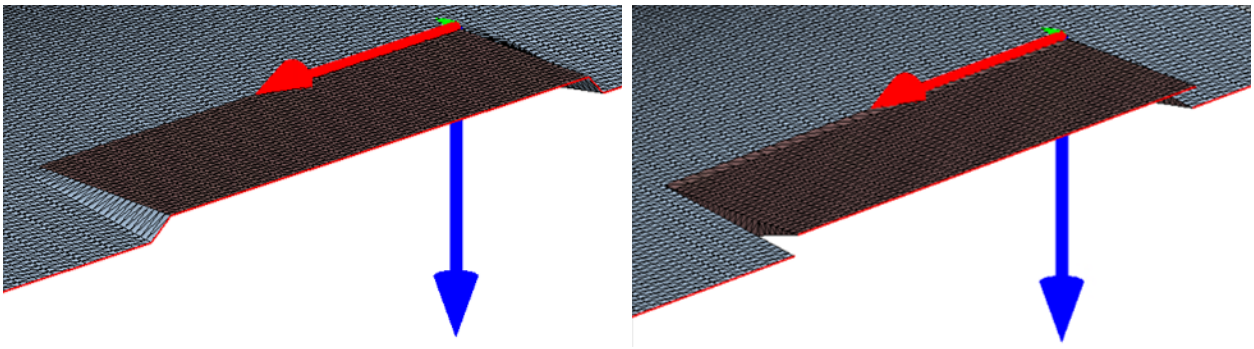

(a) Morphing control surface deflection **(b) Physical control surface deflection**

Fig. 10 Comparison of FlightStream® control surface deflection options.

Figure 11 shows a stabilator sweep comparison between the inviscid FlightStream® solution and wind-tunnel measurements. The plot shows the change in lift, drag, and pitching moment coefficients relative to zero stabilator deflection. The FlightStream® predictions show overall good agreement with the wind-tunnel data. The FlightStream® solution is seen to slightly overpredict the change in lift and pitching moment due to stabilator deflection.

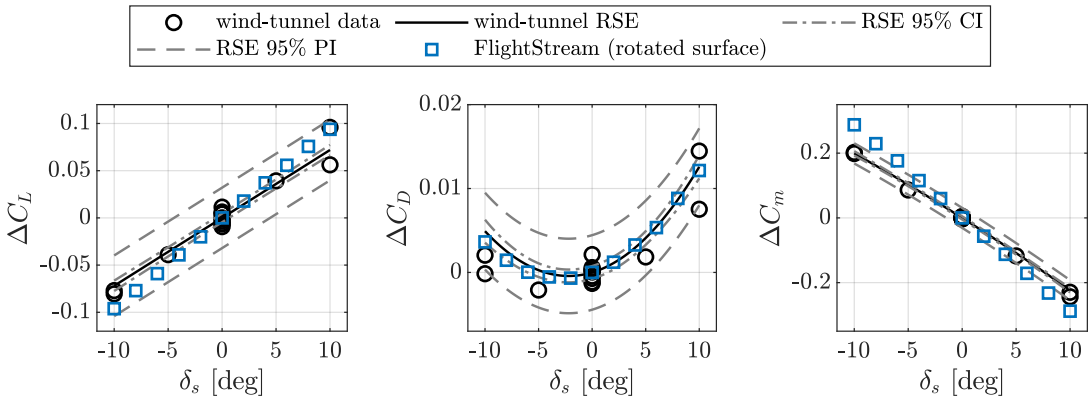

Fig. 11 Stabilator sweep at $\bar{q} = 3.5$ psf ($V = 54.3$ ft/s), $\alpha = 2$ deg, and $\beta = 0$ deg.

A rudder sweep comparison between wind-tunnel data and FlightStream® predictions for C_Y, C_l, and C_n is shown in Fig. 12. The results for morphing and physical control rudder deflection models are similar and agree well with the wind-tunnel data. The FlightStream® solution slightly overpredicts the yawing moment resulting from rudder deflection exhibited in the wind-tunnel data.

Figures 13-15 show FlightStream® left inboard, midboard, and outboard flaperon sweep predictions compared to

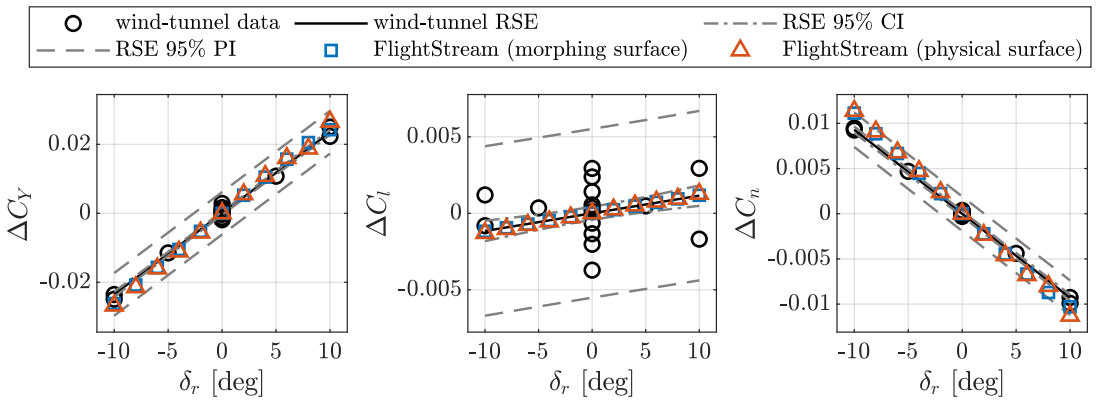

Fig. 12 Rudder sweep at $\bar{q}$ = 3.5 psf (V = 54.3 ft/s), α = 2 deg, and β = 0 deg.

wind-tunnel data for C_L, C_D, and C_l. The right wing flaperon FlightStream® predictions were nearly identical and are, thus, not shown. For this study, the morphing control surface approach yielded more reliable solutions for the flaperons and is the only deflection method shown on the plots. The outboard flaperon predictions (δ_{f_1}) agree very well with the wind-tunnel data with only a slight over-prediction of control effectiveness. The midboard and inboard flaperon deflections (δ_{f_2} and δ_{f_3}) agree reasonably well with the wind-tunnel data, but overpredict the flaperon control effectiveness for lift and rolling moment production.

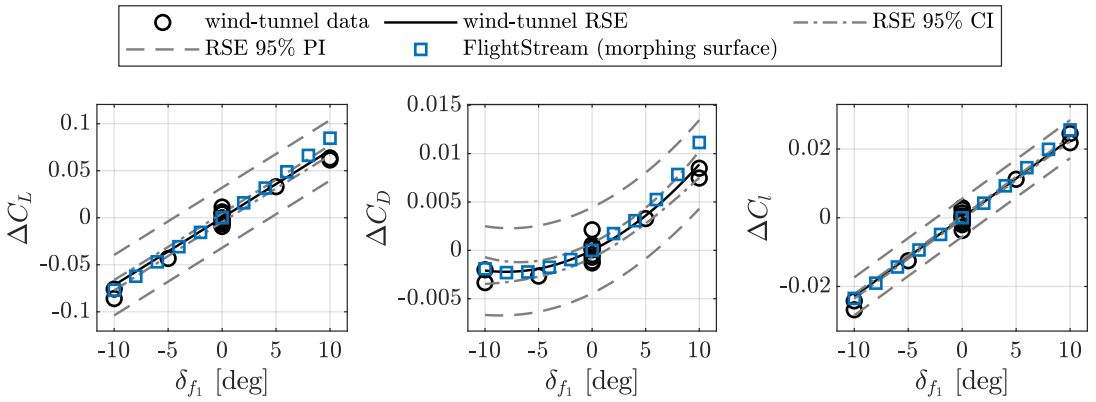

Fig. 13 Left outboard flaperon sweep at $\bar{q}$ = 3.5 psf (V = 54.3 ft/s), α = 2 deg, and β = 0 deg.

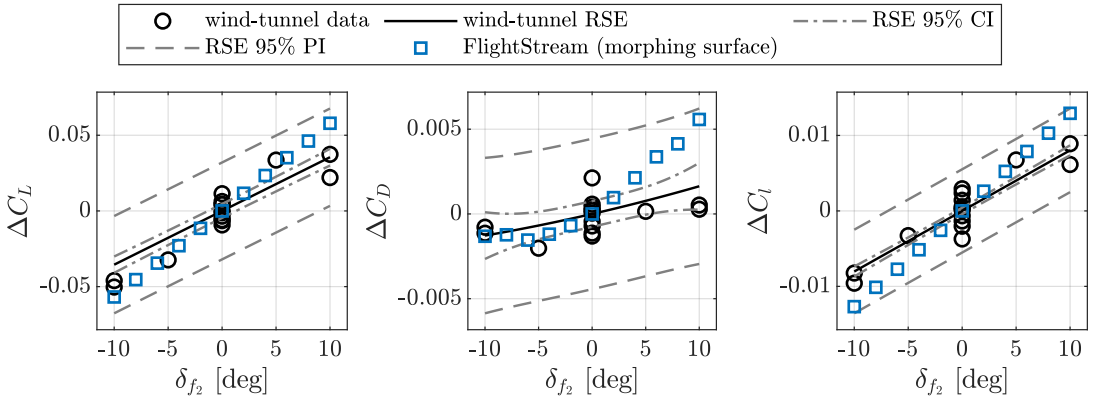

Fig. 14 Left midboard flaperon sweep at $\bar{q}$ = 3.5 psf (V = 54.3 ft/s), α = 2 deg, and β = 0 deg.

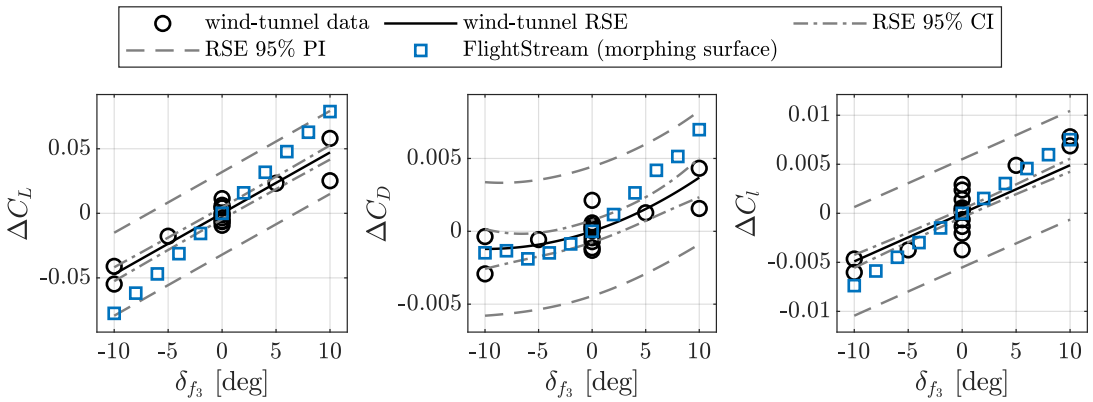

Fig. 15 Left inboard flaperon sweep at $\bar{q}$ = 3.5 psf (V = 54.3 ft/s), α = 2 deg, and β = 0 deg.

The control derivatives at $\alpha = 2$ deg and $\beta = 0$ deg computed from the wind-tunnel-derived RSEs and FlightStream® predictions using a smoothed polynomial representation of the data are shown in Table 3. The FlightStream® control derivative computations are for the morphing rudder and morphing flaperon predictions. The FlightStream® control derivative predictions are seen to overpredict the control effectiveness compared to the wind-tunnel-derived values, as would be expected from an inviscid flow solution. However, given the low computational expense of the mid-fidelity aerodynamic prediction tool, the FlightStream® control derivative predictions are acceptably close to the wind-tunnel results.

Table 3 Comparison of control derivatives at $\bar{q}$ = 3.5 psf (V = 54.3 ft/s), α = 2 deg, and β = 0 deg

Parameter	Wind Tunnel	FlightStream
$C_{L_{\delta_s}}$	+0.412	+0.548
$C_{D_{\delta_s}}$	+0.0220	+0.0274
$C_{m_{\delta_s}}$	-1.21	-1.65
$C_{Y_{\delta_r}}$	+0.135	+0.152
$C_{l_{\delta_r}}$	+0.00661	+0.00680
$C_{n_{\delta_r}}$	-0.0533	-0.0647
$C_{L_{\delta_{f_1}}}$	+0.411	+0.450
$C_{D_{\delta_{f_1}}}$	+0.0314	+0.0349
$C_{l_{\delta_{f_1}}}$	+0.131	+0.135
$C_{L_{\delta_{f_2}}}$	+0.203	+0.332
$C_{D_{\delta_{f_2}}}$	+0.00834	+0.0238
$C_{l_{\delta_{f_2}}}$	+0.0460	+0.0745
$C_{L_{\delta_{f_3}}}$	+0.270	+0.452
$C_{D_{\delta_{f_3}}}$	+0.0140	+0.0293
$C_{l_{\delta_{f_3}}}$	+0.0281	+0.0432

C. Dynamic Derivative Predictions

FlightStream® can be used to predict dynamic derivatives using both its Stability and Control Toolbox and by setting a rotational flowfield. The later approach was used for this work so that a sweep of rotation rates about the aircraft center of gravity location could be collected. The results generally agreed with physical intuition, but are not shown because wind-tunnel data was not used to validate the predictions. Future dynamic wind-tunnel testing is expected to

yield dynamic derivative values that can be compared to FlightStream® predictions.

VI. Conclusions

FlightStream®, a mid-fidelity surface-vorticity flow solver, was employed to predict the variation of aerodynamic force and moment coefficients with airflow angles, angular rates, and control surface deflection angles to analyze aircraft performance, stability, and control characteristics. The analysis approach was applied to the RAVEN SWFT aircraft in its isolated-airframe configuration. The FlightStream® results were compared to static wind-tunnel data collected for the RAVEN SWFT aircraft. The general character of the FlightStream® predictions agree well with the wind-tunnel data. The computational predictions were deemed a sufficiently accurate representation of the actual aircraft aerodynamics, prefaced with the understanding that FlightStream® is a mid-fidelity tool that yields quick flow solutions accessible early in the aircraft design process. Given the suitable results obtained for the isolated airframe, future work seeks to apply and refine the approach for the RAVEN SWFT powered airframe, as well as other eVTOL aircraft configurations, to enable development of aero-propulsive models intended for use in flight dynamics simulations. Future work is also expected to include using the FlightStream® viscous coupling settings, validation of dynamic derivative predictions, and enhancement of the range of applicability and accuracy for control surface deflection predictions.

Acknowledgments

This research was funded by the NASA Aeronautics Research Mission Directorate (ARMD) Transformational Tools and Technologies (TTT) project and Convergent Aeronautics Solutions (CAS) project. Wind-tunnel test support was provided by Ronald Busan, Wes O'Neal, Gregory Howland, Matthew Gray, Neil Coffey, Clinton Duncan, Earl Harris, and Richard Thorpe.

References

[1] Johnson, W., Silva, C., and Solis, E., "Concept Vehicles for VTOL Air Taxi Operations," *AHS Technical Conference on Aeromechanics Design for Transformative Vertical Flight*, Jan. 2018.

[2] Silva, C., Johnson, W., Antcliff, K. R., and Patterson, M. D., "VTOL Urban Air Mobility Concept Vehicles for Technology Development," *2018 Aviation Technology, Integration, and Operations Conference*, AIAA Paper 2018-3847, Jun. 2018. https://doi.org/10.2514/6.2018-3847.

[3] Saeed, A. S., Younes, A. B., Cai, C., and Cai, G., "A survey of hybrid Unmanned Aerial Vehicles," *Progress in Aerospace Sciences*, Vol. 98, 2018, pp. 91–105. https://doi.org/10.1016/j.paerosci.2018.03.007.

[4] Kim, H. D., Perry, A. T., and Ansell, P. J., "A Review of Distributed Electric Propulsion Concepts for Air Vehicle Technology," *2018 AIAA/IEEE Electric Aircraft Technologies Symposium*, AIAA Paper 2018-4998, Jul. 2018. https://doi.org/10.2514/6.2018-4998.

[5] Johnson, W., and Silva, C., "NASA Concept Vehicles and the Engineering of Advanced Air Mobility Aircraft," *The Aeronautical Journal*, Vol. 126, No. 1295, 2022, pp. 59–91. https://doi.org/10.1017/aer.2021.92.

[6] Murphy, P. C., Buning, P. G., and Simmons, B. M., "Rapid Aero Modeling for Urban Air Mobility Aircraft in Computational Experiments," *AIAA SciTech 2021 Forum*, AIAA Paper 2021-1002, Jan. 2021. https://doi.org/10.2514/6.2021-1002.

[7] Simmons, B. M., Buning, P. G., and Murphy, P. C., "Full-Envelope Aero-Propulsive Model Identification for Lift+Cruise Aircraft Using Computational Experiments," *AIAA AVIATION 2021 Forum*, AIAA Paper 2021-3170, Aug. 2021. https://doi.org/10.2514/6.2021-3170.

[8] Busan, R. C., Rothhaar, P. M., Croom, M. A., Murphy, P. C., Grafton, S. B., and O'Neal, A. W., "Enabling Advanced Wind-Tunnel Research Methods Using the NASA Langley 12-Foot Low Speed Tunnel," *14th AIAA Aviation Technology, Integration, and Operations Conference*, AIAA Paper 2014-3000, Jun. 2014. https://doi.org/10.2514/6.2014-3000.

[9] Murphy, P. C., and Landman, D., "Experiment Design for Complex VTOL Aircraft with Distributed Propulsion and Tilt Wing," *AIAA Atmospheric Flight Mechanics Conference*, AIAA Paper 2015-0017, Jan. 2015. https://doi.org/10.2514/6.2015-0017.

[10] Murphy, P. C., Simmons, B. M., Hatke, D. B., and Busan, R. C., "Rapid Aero Modeling for Urban Air Mobility Aircraft in Wind-Tunnel Tests," *AIAA SciTech 2021 Forum*, AIAA Paper 2021-1644, Jan. 2021. https://doi.org/10.2514/6.2021-1644.

[11] Busan, R. C., Murphy, P. C., Hatke, D. B., and Simmons, B. M., "Wind Tunnel Testing Techniques for a Tandem Tilt-Wing, Distributed Electric Propulsion VTOL Aircraft," *AIAA SciTech 2021 Forum*, AIAA Paper 2021-1189, Jan. 2021. https://doi.org/10.2514/6.2021-1189.

[12] Simmons, B. M., and Murphy, P. C., "Aero-Propulsive Modeling for Tilt-Wing, Distributed Propulsion Aircraft Using Wind Tunnel Data," *Journal of Aircraft*, Vol. 59, No. 5, 2022, pp. 1162–1178. https://doi.org/10.2514/1.C036351.

[13] Simmons, B. M., Morelli, E. A., Busan, R. C., Hatke, D. B., and O'Neal, A. W., "Aero-Propulsive Modeling for eVTOL Aircraft Using Wind Tunnel Testing with Multisine Inputs," *AIAA AVIATION 2022 Forum*, AIAA Paper 2022-3603, Jun. 2022. https://doi.org/10.2514/6.2022-3603.

[14] Cook, J. W., and Hauser, J., "A Strip Theory Approach to Dynamic Modeling of eVTOL Aircraft," *AIAA SciTech 2021 Forum*, AIAA Paper 2021-1720, Jan. 2021. https://doi.org/10.2514/6.2021-1720.

[15] May, M. S., Milz, D., and Looye, G., "Dynamic Modeling and Analysis of Tilt-Wing Electric Vertical Take-Off and Landing Vehicles," *AIAA SciTech 2022 Forum*, AIAA Paper 2022-0263, San Diego, CA & Virtual, Jan. 2022. https://doi.org/10.2514/6.2022-0263.

[16] Perdolt, D., Milz, D., May, M., and Thiele, M., "Efficient Mid-Fidelity Aerodynamic Modeling of a Tilt-Wing eVTOL for Control Applications," *33th Congress of the International Council of the Aeronautical Sciences*, ICAS Paper 2022-0860, Sep. 2022.

[17] May, M. S., Milz, D., and Looye, G., "Semi-Empirical Aerodynamic Modeling Approach for Tandem Tilt-Wing eVTOL Control Design Applications," *AIAA SciTech 2023 Forum*, AIAA Paper 2023-1529, Jan. 2023. https://doi.org/10.2514/6.2023-1529.

[18] Chakraborty, I., and Mishra, A. A., "Sizing and Analysis of a Lift-Plus-Cruise Aircraft with Electrified Propulsion," *Journal of Aircraft*, Published online 31 October 2022, pp. 1–19 (Article in Advance). https://doi.org/10.2514/1.C037044.

[19] Comer, A. M., and Chakraborty, I., "Total Energy Flight Control Architecture Optimization for a Lift-Plus-Cruise Aircraft," *AIAA SciTech 2023 Forum*, AIAA Paper 2023-0399, Jan. 2023. https://doi.org/10.2514/6.2023-0399.

[20] "FlightStream®: Fast Aerodynamics with Fidelity," *Research in Flight*, https://researchinflight.com/index.html, Accessed 29 October 2022.

[21] Sandoz, B., Ahuja, V., and Hartfield, R. J., "Longitudinal Aerodynamic Characteristics of a V/STOL Tilt-wing Four-Propeller Transport Model using a Surface Vorticity Flow Solver," *2018 AIAA Aerospace Sciences Meeting*, AIAA Paper 2018-2070, Jan. 2018. https://doi.org/10.2514/6.2018-2070.

[22] Blaesser, N. J., "Propeller-Wing Integration on the Parallel Electric-Gas Architecture with Synergistic Utilization Scheme (PEGASUS) Aircraft," *AIAA SciTech 2019 Forum*, AIAA Paper 2019-1809, Jan. 2019. https://doi.org/10.2514/6.2019-1809.

[23] Hartfield, R. J., Ahuja, V., and Chakraborty, I., "Aero-Propulsive Analysis for Contemporary Conceptual Design," *AIAA Aviation 2019 Forum*, AIAA Paper 2019-3019, June 2019. https://doi.org/10.2514/6.2019-3019.

[24] Fei, X., "Evaluation of a Commercial Surface Vorticity Flow Solver for the Modeling of Propeller-Wing Interaction," *AIAA SciTech 2019 Forum*, AIAA Paper 2019-1046, Jan. 2019. https://doi.org/10.2514/6.2019-1046.

[25] Chakraborty, I., Ahuja, V., Comer, A., and Mulekar, O., "Development of a Modeling, Flight Simulation, and Control Analysis Capability for Novel Vehicle Configurations," *AIAA Aviation 2019 Forum*, AIAA Paper 2019-3112, Jun. 2019. https://doi.org/10.2514/6.2019-3112.

[26] Soikkeli, J. S. E., "Vertical Tail Reduction Through Differential Thrust," Master's thesis, Delft University of Technology, Mar. 2020.

[27] Geuther, S. C., and Fei, X., "LA-8 Computational Analysis and Validation Studies Using FlightStream," *AIAA SciTech 2021 Forum*, AIAA Paper 2021-1191, Jan. 2021. https://doi.org/10.2514/6.2021-1191.

[28] Hoogreef, M. F. M., and Soikkeli, J. S. E., "Flight dynamics and control assessment for differential thrust aircraft in engine inoperative conditions including aero-propulsive effects," *CEAS Aeronautical Journal*, Vol. 13, No. 3, 2022, pp. 739–762. https://doi.org/10.1007/s13272-022-00591-5.

[29] Ahuja, V., and Litherland, B. L., "Comparison of Aerodynamic Analysis Tools Applied to a Propeller-Blown Wing," *AIAA SciTech 2023 Forum*, AIAA Paper 2023-1753, Jan. 2023. https://doi.org/10.2514/6.2023-1753.

[30] Ahuja, V., and Hartfield, R. J., "Aerodynamic Loads over Arbitrary Bodies by Method of Integrated Circulation," *Journal of Aircraft*, Vol. 53, No. 6, 2016, pp. 1719–1730. https://doi.org/10.2514/1.C033619.

[31] Olson, E. D., and Albertson, C. W., "Aircraft High-Lift Aerodynamic Analysis Using a Surface-Vorticity Solver," *54th AIAA Aerospace Sciences Meeting*, AIAA Paper 2016-0779, Jan. 2016. https://doi.org/10.2514/6.2016-0779.

[32] Johnson, S., Hartfield, R. J., van Dommelen, D., and Ahuja, V., "Investigation of the Static Longitudinal Characteristics of a Full-Scale Light Single-Engine Airplane using a Surface Vorticity Solver," *2018 AIAA Aerospace Sciences Meeting*, AIAA Paper 2018-1259, Jan. 2018. https://doi.org/10.2514/6.2018-1259.

[33] Ahuja, V., Little, D. S., Majdalani, J., and Hartfield, R., "Integrated Computational Aeroacoustics for UAM Design. Part 1. Farassat F1A Formulation," *AIAA AVIATION 2022 Forum*, AIAA Paper 2022-3954, Jun. 2022. https://doi.org/10.2514/6.2022-3954.

[34] Pastor, G., Hartfield, R., and Ahuja, V., "Expedited Solutions for Propeller Analysis," *AIAA SciTech 2022 Forum*, AIAA Paper 2022-1158, Jan. 2022. https://doi.org/10.2514/6.2022-1158.

[35] DiMaggio, G. A., Hartfield, R. J., and Ahuja, V., "Rapid Prediction of Hybrid Wing Body Aerodynamics," *AIAA AVIATION 2022 Forum*, AIAA Paper 2022-3298, Jun. 2022. https://doi.org/10.2514/6.2022-3298.

[36] Pastor, G., Hartfield, R., Ahuja, V., and McClearen, J., "Numerical and Experimental Testing of a Coaxial Propeller for UAM Applications," *AIAA AVIATION 2022 Forum*, AIAA Paper 2022-3683, Jun. 2022. https://doi.org/10.2514/6.2022-3683.

[37] Ahuja, V., and Hartfield, R. J., "Reduced-Order Aerodynamics with the Method of Integrated Circulation," *AIAA SciTech 2022 Forum*, AIAA Paper 2022-0005, Jan. 2022. https://doi.org/10.2514/6.2022-0005.

[38] Collins, W. F., Hartfield, R. J., and Ahuja, V., "Pressure Distributions for Bodies of Revolution in Compressible Flows Using an Advanced Panel Method," *AIAA SciTech 2023 Forum*, AIAA Paper 2023-2271, 2023. https://doi.org/10.2514/6.2023-2271.

[39] Ahuja, V., Hartfield, R. J., and Ciliberti, D., "Three-dimensional Viscous Coupling & Flow Separation Enhancements to an Inviscid Surface Vorticity Flow Solver," *AIAA SciTech 2023 Forum*, AIAA Paper 2023-2455, National Harbor, MD & Online, 2023. https://doi.org/10.2514/6.2023-2455.

[40] DiMaggio, G. A., Hartfield, R. J., and Ahuja, V., "Hybrid Wing Body Pitch Control with a Surface-Vorticity Solver," *AIAA SciTech 2023 Forum*, AIAA Paper 2023-0623, Jan. 2023. https://doi.org/10.2514/6.2023-0623.

[41] Wang, X., Hartfield, R. J., and Ahuja, V., "Prediction of Duct Airfoil Aerodynamics using Surface Vorticity," *AIAA SciTech 2023 Forum*, AIAA Paper 2023-1949, Jan. 2023. https://doi.org/10.2514/6.2023-1949.

[42] German, B. J., Jha, A., Whiteside, S. K. S., and Welstead, J. R., "Overview of the Research Aircraft for eVTOL Enabling techNologies (RAVEN) Activity," *AIAA AVIATION 2023 Forum*, June 2023. To be published.

[43] "NASA Langley 12-Foot Low-Speed Tunnel," https://researchdirectorate.larc.nasa.gov/12-foot-low-speed-tunnel-12-ft-lst/, Accessed 18 April 2023.

[44] McSwain, R. G., Geuther, S. C., Howland, G., Patterson, M. D., Whiteside, S. K., and North, D. D., "An Experimental Approach to a Rapid Propulsion and Aeronautics Concepts Testbed," NASA TM–2020-220437, Jan. 2020.

[45] North, D. D., Busan, R. C., and Howland, G., "Design and Fabrication of the Langley Aerodrome No. 8 Distributed Electric Propulsion VTOL Testbed," *AIAA SciTech 2021 Forum*, AIAA Paper 2021-1188, Jan. 2021. https://doi.org/10.2514/6.2021-1188.

[46] Rothhaar, P. M., Murphy, P. C., Bacon, B. J., Gregory, I. M., Grauer, J. A., Busan, R. C., and Croom, M. A., "NASA Langley Distributed Propulsion VTOL Tilt-Wing Aircraft Testing, Modeling, Simulation, Control, and Flight Test Development," *14th AIAA Aviation Technology, Integration, and Operations Conference*, AIAA Paper 2014-2999, Jun. 2014. https://doi.org/10.2514/6.2014-2999.

[47] Geuther, S. C., North, D. D., and Busan, R. C., "Investigation of a Tandem Tilt-wing VTOL Aircraft in the NASA Langley 12-Foot Low-Speed Tunnel," NASA TM–2020–5003178, Jun. 2020.

[48] Simmons, B. M., and Hatke, D. B., "Investigation of High Incidence Angle Propeller Aerodynamics for Subscale eVTOL Aircraft," NASA TM–20210014010, May 2021.

[49] Simmons, B. M., "System Identification for Propellers at High Incidence Angles," *Journal of Aircraft*, Vol. 58, No. 6, 2021, pp. 1336–1350. https://doi.org/10.2514/1.C036329.

[50] Stratton, M., and Landman, D., "Wind Tunnel Test and Empirical Modeling of Tilt-Rotor Performance for eVTOL Applications," *AIAA SciTech 2021 Forum*, AIAA Paper 2021-0834, Jan. 2021. https://doi.org/10.2514/6.2021-0834.

[51] Simmons, B. M., "Evaluation of Response Surface Experiment Designs for Distributed Propulsion Aircraft Aero-Propulsive Modeling," *AIAA SciTech 2023 Forum*, AIAA Paper 2023-2251, Jan. 2023. https://doi.org/10.2514/6.2023-2251.

[52] Cooper, J. R., Ackerman, K. A., Rothhaar, P. M., and Gregory, I. M., "Autonomous Path-Following for a Tilt-Wing, Distributed Electric Propulsion, Vertical Take-Off and Landing Unmanned Aerial System in Hover Mode," NASA TM–2018–220109, Nov. 2018.

[53] Cook, J., and Gregory, I., "A Robust Uniform Control Approach for VTOL Aircraft," *VFS Autonomous VTOL Technical Meeting and Electric VTOL Symposium*, Jan. 2021.

[54] McSwain, R. G., Glaab, L. J., and Theodore, C. R., "Greased Lightning (GL-10) Performance Flight Research – Flight Data Report," NASA TM–2017–219794, Nov. 2017.

[55] Fredericks, W. J., McSwain, R. G., Beaton, B. F., Klassman, D. W., and Theodore, C. R., "Greased Lightning (GL-10) Flight Testing Campaign," NASA TM–2017–219643, Jul. 2017.

[56] North, D. D., "Flight Testing of a Scale Urban Air Mobility Technology Testbed," *AIAA SciTech 2021 Forum*, AIAA Presentation, Jan. 2021. https://ntrs.nasa.gov/citations/20205010998, Accessed 17 October 2022.

[57] Simmons, B. M., "System Identification Approach for eVTOL Aircraft Demonstrated Using Simulated Flight Data," *Journal of Aircraft*, Published online 30 January 2023, pp. 1–16 (Article in Advance). https://doi.org/10.2514/1.C036896.

[58] Simmons, B. M., "Efficient Variable-Pitch Propeller Aerodynamic Model Development for Vectored-Thrust eVTOL Aircraft," *AIAA AVIATION 2022 Forum*, AIAA Paper 2022-3817, Jun. 2022. https://doi.org/10.2514/6.2022-3817.

[59] Ahuja, V., Burkhalter, J., and Hartfield, R., "Robust Prediction of High Lift Using Surface Vorticity," NASA Small Business Innovative Research (SBIR) Contract Award, Phase II, NNX17CL12C, 2017.

[60] Ahuja, V., Chakraborty, I., and Hartfield, R., "Modular Generalized Framework for Assessing Aircraft Aero-Propulsive, Stability, and Control Characteristics," NASA Transformational Tools & Technologies Transformative (TTT) Aeronautics Concepts Program Award, 80LARC19C0013, 2018-2021.

[61] Ahuja, V., Chakraborty, I., and Hartfield, R., "Air Vehicle Gust Response Analysis for Early Design," NASA Small Business Innovative Research (SBIR) Contract Award, Phase II, 80NSSC21C0025, 2020-2022.

[62] Ahuja, V., Hunsaker, D., and Hartfield, R., "A Rapid Aerodynamic Prediction Tool for Maneuvering Hypersonic Air Vehicles," USAF AFWERX Small Business Innovative Research (SBIR) Contract Award, Phase I, FX22D-OTCSO1-0129, 2022.

[63] Ahuja, V., Hunsaker, D., and Hartfield, R., "A Multi-Fidelity Supersonic Flow Solver for Preliminary Design & Optimization," USAF AFWERX Small Business Innovative Research (SBIR) Contract Award, Phase II, FA864922P0081, 2023.

[64] "OpenVSP," https://openvsp.org/, Version 3.31.1.

[65] McDonald, R. A., and Gloudemans, J. R., "Open Vehicle Sketch Pad: An Open Source Parametric Geometry and Analysis Tool for Conceptual Aircraft Design," *AIAA SciTech 2022 Forum*, AIAA Paper 2022-0004, Jan. 2022. https://doi.org/10.2514/6.2022-0004.

[66] Haimes, R., and Dannenhoffer, J., "The Engineering Sketch Pad: A Solid-Modeling, Feature-Based, Web-Enabled System for Building Parametric Geometry," *21st AIAA Computational Fluid Dynamics Conference*, AIAA Paper 2013-3073, June 2013. https://doi.org/10.2514/6.2013-3073.

[67] "FlightStream User Guide," *Research in Flight*, Version 2021.2.

[68] Conway, J. T., "Analytical Solutions for the Actuator Disk with Variable Radial Distribution of Load," *Journal of Fluid Mechanics*, Vol. 297, 1995, pp. 327–355. https://doi.org/10.1017/S0022112095003120.

[69] Montgomery, D. C., *Design And Analysis of Experiments*, 8th ed., John Wiley & Sons, Inc., Hoboken, NJ, 2013.

[70] Myers, R. H., Montgomery, D. C., and Anderson-Cook, C. M., *Response Surface Methodology: Process and Product Optimization Using Designed Experiments*, 4th ed., John Wiley & Sons, 2016.